analytical chemistry

pubs.acs.org/ac Letter

Intramolecular Photoelectrochemical System Using Tyrosine-Modified Antibody-Targeted Peptide as Electron Donor for Detection of Biomarkers

Shanghua Liu, Yue Jia, Hui Dong, Xiaodong Yu, Dao-Peng Zhang, Xiang Ren, Yueyun Li,* and Qin Wei*

Cite This: *Anal. Chem.* 2020, 92, 10935−10939 Read Online

ACCESS | Metrics & More | Article Recommendations | Supporting Information

ABSTRACT: An intramolecular photoelectrochemical (PEC) system is designed from the novel electron donor YYYHWRGWV (Y3-H) peptide ligand for the first time. The bifunctional nonapeptide cannot only rely on the HWRGWV sequence as a site-oriented immobilizer to recognize the crystallizable fragment (Fc) domains of the antibody but also acts as electron donors for PEC generation via three tyrosine (Y) of the N-terminal. The $Bi_2WO_6/AgInS_2$ heterojunction with a significant visible-light absorption is utilized as a photoelectric generator, and the motivation is ascribed to a proven proposition, namely, that short-wavelength illuminant radiates proteins, causing a decline in bioactivity of immune protein. An innovative biosensor is fabricated using the above strategies for the detection of CYFRA21-1, a biomarker of squamous cell lung carcinoma. This sort of PEC-based sensing platform shows convincing experimental data and could be an effective candidate for clinical application in the future due to their extremely skillful conception.

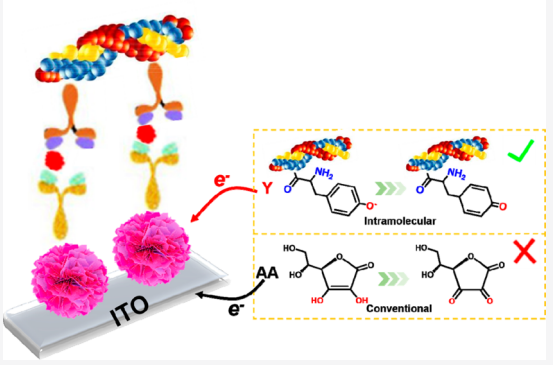

Photoelectrochemical (PEC) bioanalysis, acquainted as an advanced mean that can convert biorecognition into readable photocurrent, has become an eye-catching tool in analytical chemistry.[1] The research and development potential of PEC-based biosensors are profit from their unique signal transfer mechanism, which can be optimized through the choice of efficient photoelectric emitters and sensing strategies.[2] For photoactive materials, the application of them in biosensing at the core of care requires choosing the semiconductors with excellent biocompatibility and visible-light absorption.[1,3] The inevitable toxicity of cadmium-based compounds and other toxic carriers are distinctly unacceptable for trace analysis based on nontoxic physiology.[4]

Bismuth tungstate (Bi_2WO_6), one of the simplest orthorhombic crystals in the Aurivillius family, is a lamination of $[Bi_2O_2]$ layers and $[WO_6]$ octahedrons alternately along the *c*-direction.[5] Its valence band (VB) is mainly composed via hybridization between the O 2p and Bi 6s orbitals, while the conduction band (CB) is composed of the W 5d energy level, all that make the photoexcited electrons transfer from the O 2p/Bi 6s hybridization orbital to the empty orbital of W 5d, resulting in forming photoinduced electron−hole (e^-/h^+) pairs.[6] The lone electron pair root in the Bi 6s orbital can bring about asymmetric coordination of the Bi−W−O structure, whereas the local asymmetry charge can excite the photoelectric activity of Bi_2WO_6.[7] Limited by the narrow spectral response, there is no doubt that poses a major challenge of the expansion Bi_2WO_6 to biosensing because the protein can undergo irreversible ultraviolet radiation when the illuminant wavelength is excessively short.[8] To enhance the response of visible light, some amplified approaches and innovatory strategies should be introduced.[9]

Heterojunctions formed by mass surface contact of two semiconductors with different work functions or chemical potentials can enhance the charge separation ability of the photoelectric system and visible light response.[10,11] Quantum dots (QDs) are an excellent candidate sensitizer benefiting from their high dispersion and narrow band gap.[12] Among the multitudinous QDs, indium sulfide silver ($AgInS_2$) as a nontoxic emerging material has become one of the most promising photoelectric sensitizers to rely on an adjustable direct band gap.[13] With plentiful surface defects, the heterojunction between $AgInS_2$ and other semiconductors can easily form via raised surface energy and dangling bonds.[14]

Received: June 30, 2020
Accepted: August 4, 2020
Published: August 4, 2020

https://dx.doi.org/10.1021/acs.analchem.0c02804
Anal. Chem. 2020, 92, 10935−10939

In the past, plenty of ascorbic acids (AA) are usually injected into the electrolyte to meet the stability of the whole test.[15,16] Nevertheless, this sensing mode relies on the resistance of antigen to the electron transfer to obtain the inverse relationship between target concentration and photocurrent, which is unreasonable for sensitive detection. The photocurrent response has almost no difference when the target concentration is small enough that its resistance can be ignored. Otherwise, the coexistence of AA and other reducing substances in serum also undoubtedly weakens the anti-interference of the biosensor. Alternative approaches of the electron donor external-injection are being explored, for instance, tyrosine (Y) as an intramolecular donor, which equips a side chain of phenol. When pH is amplified to 9.8 or higher, phenolic hydroxyl loses proton to form intermediate-state phenoxyanion (p-O^-) with considerable reducibility.[17,18] Foremost, this substance might be coupled as well to synthesize functional peptides in line with targeted demand, such as small molecule peptide ligand for antibody site-fixated or cell recognition.[19,20] With a fixed transportation route, all electrons can be transported orderly from the secondary antibody marker to the PEC emitter.

Herein, a long-term proposition is first proved by circular dichroism (CD) spectra, namely, that short-wavelength illuminant radiates proteins, causing a decline in immune protein bioactivity; the detailed process of proof is shown in section SI-9 in the Supporting Information for better understanding. Based on this fact, $AgInS_2$ QDs are embedded in the aperture of the Bi_2WO_6 microsphere for the construction of heterojunction (Bi_2WO_6/$AgInS_2$) to improve visible-light utilization and e^-/h^+ pairs separation. Scheme 1 stands for the energy band structure of Bi_2WO_6/$AgInS_2$ composites and the PEC mechanism using Y as an the electron donor. The power producer of carriers transfer roots in the matched interlacing band gap of Bi_2WO_6 and $AgInS_2$. Influenced by the van der Waals force, the heterojunction interface is formed gradually with the Bi_2WO_6 and $AgInS_2$ energy bands upshifting or downshifting until the Fermi energy level attains equilibrium. In accordance with the law of thermodynamic equilibrium, the photoexcited electrons in the CB of $AgInS_2$ can easily jump to the CB of Bi_2WO_6 via a large number of Bi−S bonds in the heterojunction interface. While photoexcited holes could be driven from the VB of Bi_2WO_6 to $AgInS_2$, carrier cycles mirror the same path at a site opposite to the electron transfer. The addition of p-O^- as the electron donor can rapidly consume the holes in the whole system to restrain the recombination of the e^-/h^+ pairs, thus amplifying the photoelectric response. The increased photocurrent of Bi_2WO_6/$AgInS_2$ composites as compared to pure Bi_2WO_6 confirms the above theoretical prediction (Figure S2).

Scheme 1. PEC Mechanism of Bi_2WO_6/$AgInS_2$ Heterojunction and Graphical Expression of e^-/h^+ Separation Using Y as an Electron Donor

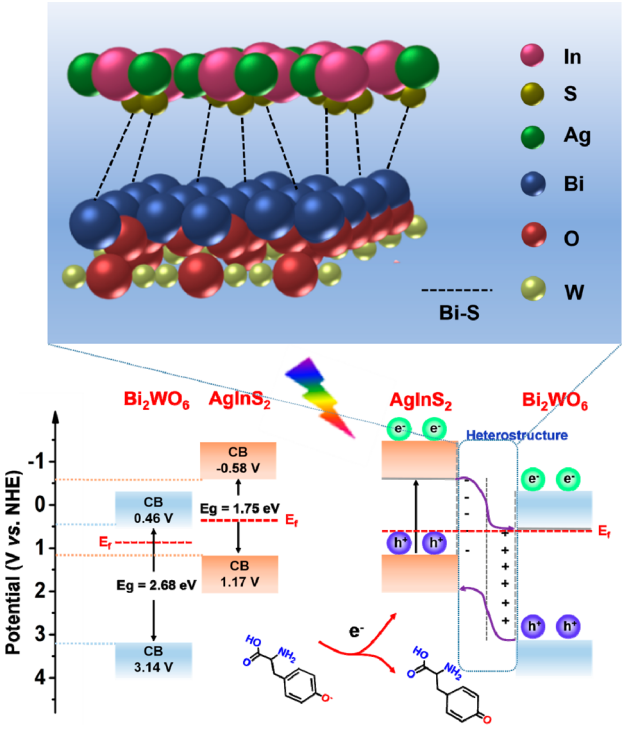

The X-ray diffraction (XRD) patterns of as-synthesized Bi_2WO_6 and Bi_2WO_6/$AgInS_2$ are provided in Figure 1a.

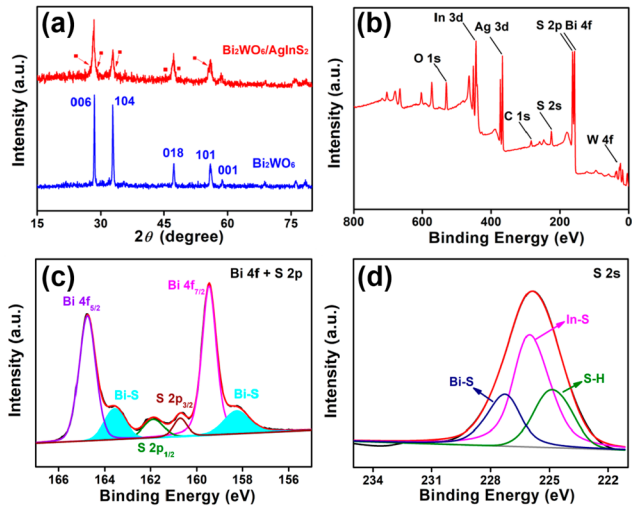

Figure 1. (a) XRD patterns of Bi_2WO_6 and Bi_2WO_6/$AgInS_2$ and (b) XPS overall spectrum of Bi_2WO_6/$AgInS_2$. High-resolution XPS spectra of Bi 4f and S 2p (c) and S 2s (d).

Compared with the pure Bi_2WO_6, Bi_2WO_6/$AgInS_2$ emerges multiple low peaks that are not obvious at 2-theta = 27.42°, 28.97°, 33.15°, 46,74°, 48.27°, and 55.04°, which belong to the characteristic peak of $AgInS_2$ are corresponding to (006), (012), (104), (018), (110), and (101) lattice planes (JCPDS card no. 22-1329 and no. 39-0256).[21] To further confirm the existence of $AgInS_2$ to make up for the defects of the XRD pattern, the X-ray photoelectron spectroscopy (XPS) is used for analysis of the valence state of the composites, from which the composition of heterojunctions are well elucidated. The overall survey of the XPS spectrum, displayed in Figure 1b, illustrates the existent of Bi, W, O, Ag, In, and S elements. The spin−orbit components of Bi $4f_{7/2}$ and Bi $4f_{5/2}$ peaks are shifted to approximate 159.4 and 164.7 eV (Figure 1c), respectively. The distinct movement compared to the standard peaks is likely a result of the formation of Bi−S bonds, which can be proved via shoulder satellite peaks at 158.3 and 163.5 eV.[22,23] Besides, the peaks that situate at 226.0 and 227.3 eV split from the S 2s fitting spectrum are assigned to the sulfur in metal−sulfur bonds of In−S and Bi−S, while the peak located at 224.5 eV is the residual sulfydryl root in dodecyl mercaptan

https://dx.doi.org/10.1021/acs.analchem.0c02804
Anal. Chem. 2020, 92, 10935−10939

(Figure 1d).[24,25] All of these, along with other core level XPS spectra (see section SI-11 in the Supporting Information), confirming the successful preparation of Bi_2WO_6/$AgInS_2$ composites.

To probe into the morphological feature of Bi_2WO_6, $AgInS_2$, and their composites, the scanning electron microscope (SEM) and transmission electron microscope (TEM) images are provided in Figure 2. Flower-shaped Bi_2WO_6 (Figure 2a and

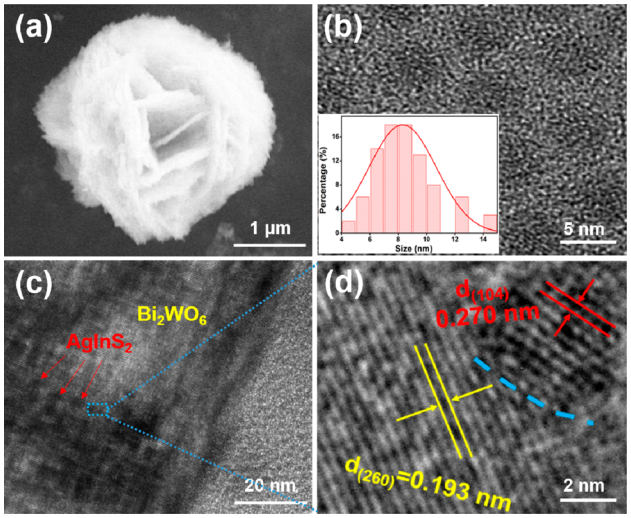

Figure 2. (a) SEM image of Bi_2WO_6, (b) TEM image and size distribution of $AgInS_2$ QDs, and (c) TEM and (d) HRTEM images of Bi_2WO_6/$AgInS_2$ composites.

Figure S4a) microspheres inserted by countless nanosheets provides a mass of attached spaces for $AgInS_2$ immobilization. Later, both TEM image and size distribution of $AgInS_2$ QDs show a uniform particle size of about 8 ± 1 nm (Figure 2b). After inlay in Bi_2WO_6, the $AgInS_2$ QDs equally disperse on Bi_2WO_6 nanosheet observed from the TEM (Figure 2c). To confirm the successful heterojunction formation, the high-resolution TEM (HRTEM) observes the different lattice configurations (Figure 2d) and has no buffer layers or amorphous phase between Bi_2WO_6 and $AgInS_2$. All of that provide strong evidence that the Bi_2WO_6/$AgInS_2$ heterojunction is successfully fabricated owing to such lattice distribution is recognized as typical heterojunctions, corresponding to the XPS and UV−vis (see in section SI-13 in the Supporting Information) results.[26]

The expansion of the above PEC system to the immunoassay utilizing Bi_2WO_6/$AgInS_2$ acting as a sensing substrate to coupling capture antibody ($anti_1$-CYFRA21-1) and functioning as a photocurrent generator realizing signal converter. Y-Modified YYYHWRGWV (Y3-H) nonapeptide, however, is used for marker detection antibody ($anti_2$-CYFRA21-1) and also provides electrons to the whole PEC system. In the past, it is obviously unreasonable to obtain the inverse relationship between signal and antigen concentration using the signal-off PEC biosensors, which rely on the hindrance of antigen to the electron. Because the impedance is negligible when the antigen concentration is low to the picogram level, that undoubtedly limits the detection range of the biosensor. Herein, bounding Y to $anti_2$-CYFRA21-1, as the concentration of antigen raises, more $anti_2$-CYFRA21-1 can be captured. In consequence, raising Y to realize the increase of the photocurrent, this signal-on mode makes up for the defects of the traditional scheme. The detailed diagram of biosensor fabrication and intramolecular PEC are illustrated in Scheme 2. (EIS profiles and photocurrent−time (I−t) curves are provided in section SI-14 in the Supporting Information for ensuring the stepwise biosensor fabrication).

Scheme 2. Detailed Diagram of Biosensor Fabrication and Intramolecular PEC

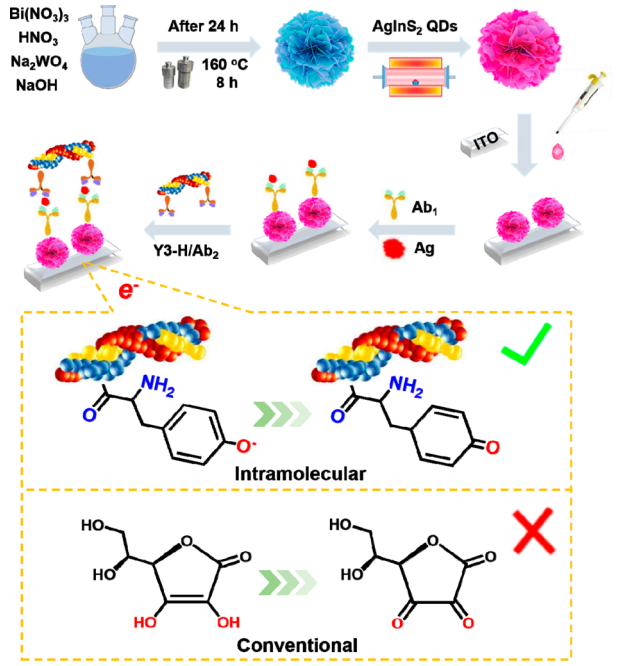

Under optimal conditions (see in section SI-15 in the Supporting Information), different concentrations of CYFRA21-1 are detected for evaluating the clinical utility of the biosensor. It can be seen from the figure that the as-fabricated biosensors have a good photoelectric response to CYFRA21-1 with a linear range of 0.5 pg mL^{-1} to 100 ng mL^{-1} (Figure 3a). With fitting, a calibration equation is obtained and described as $I = 23.81 - 94.71 \times \lg c$ with a correlation coefficient (R^2) of 0.992 (Figure S8). Later, an ultralow limit of detection (LOD) is attained that is 7.72 fg mL^{-1} (S/N = 3) lower than other reports (Table S1) according to the method suggested in Compendium of Analytical Nomenclature.

Taking into account the diversity of serum sample constituents, for instance, total cholesterol (TC), triglyceride (TG), estradiol (EZ), C-reactive protein (CRP), albumin (ALB), procalcitonin (PCT), glutamic-pyruvic transaminase (ALT), bilirubin (BIL), etc., may interfere with the real sample analysis data of the biosensor. These constant substances are selected as interferents to assess the specificity of the as-fabricated biosensor. Mixing these substances with 0.1 ng mL^{-1} CYFRA21-1 and modifying them orderly as a target on the sensing interface and detecting the photocurrent under the same conditions as before. The stable photocurrent of each sensor are summarized in Figure 3b, almost a similar photocurrent intensity with a relative standard deviation (RSD) of 1.33% proves that the biosensor has excellent specificity.

The commercialization of biosensors depends directly on their stability and batch consistency. First, to test the excitation stability of the as-fabricated biosensor, 2 equiv of antigens with

https://dx.doi.org/10.1021/acs.analchem.0c02804
Anal. Chem. 2020, 92, 10935−10939

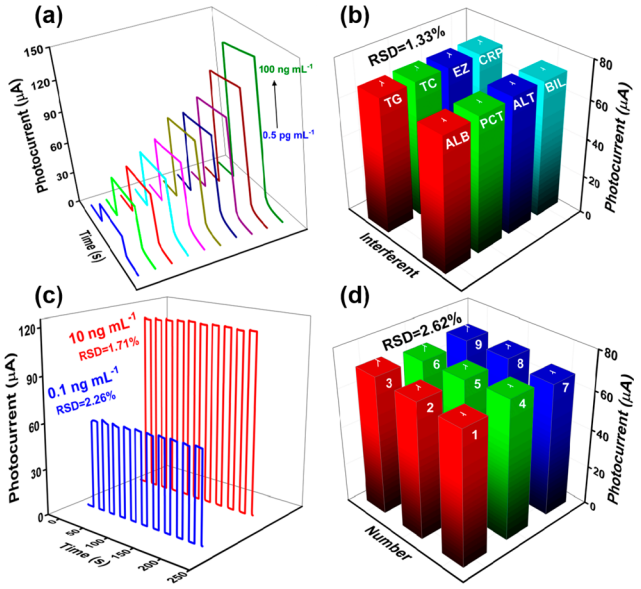

Figure 3. (a) $I-t$ curves of CYFRA21-1 detection with multiple concentrations ranging from 0.5 pg mL^{-1} to 100 ng mL^{-1}. (b) Specificity experiments of as-prepared biosensor using common substances in serum. (c) Stability experiments for low and high concentration of CYFRA21-1 using as-prepared biosensor. (d) Repeatability experiments are carried out by detecting nine biosensors modified with 0.1 ng mL^{-1} CYFRA21-1 (error bar = SD, n = 3).

0.1 ng mL^{-1} and 10 ng mL^{-1} are employed to evaluate this metric. Neither high nor low concentrations show a significant fluctuation of photocurrent signal of biosensor output (Figure 3c). Following, we repeat the experiments on nine biosensors modified with 0.1 ng mL^{-1} CYFRA21-1 under the same experimental conditions (Figure 3d). With a low RSD of 2.62, the good batch consistency provides convincing evidence for the application of clinical sensing strategies.

The sample-labeling-recovery approach is used to analyze CYFRA21-1 in human serum. To start the detection, five serum samples obtained from the school hospital with an original concentration of 0.7 ng mL^{-1} are mixed with different spikings of CYFRA21-1 as 0.5, 1, 5, 10, 50 ng mL^{-1}. Modifying them as a target and converting the current signal into CYFRA21-1 concentration, recovery rates (Rt) from 91.90% to 98.96% are obtained (Table S2) by the equation of Rt = (Found − Origin)/Spiked, proving the practicability of the as-purposed biosensor.

In summary, as a bifunctional nonapeptide, Y3-H can function not only as an intramolecular electron donor for holes consumption but able to act as a site-fixed capturer for antibody conjugation. As-purposed intramolecular PEC system using the $Bi_2WO_6/AgInS_2$ heterojunction as a photocurrent generator, which can effectively maintain the protein bioactivity in the detection process and avoid the complexity of serum samples to interfere with the detection results. With these innovative approaches for CYFRA21-1 analysis, a biomarker of squamous carcinoma, the sensing platform reveals a potential for clinical application due to its remarkable sensitivity and anti-interference ability.

■ ASSOCIATED CONTENT

Supporting Information

The Supporting Information is available free of charge at https://pubs.acs.org/doi/10.1021/acs.analchem.0c02804.

Materials and reagents; apparatus; synthesis of Bi_2WO_6; synthesis of water-soluble $AgInS_2$ QDs; preparation of $Bi_2WO_6/AgInS_2$ heterojunction; preparation of anti$_2$-CYFRA21-1/Y3-H bioconjugates; fabrication of the PEC biosensor; PEC measurements; CD analysis of protein bioactivity; photocurrent contrast between Bi_2WO_6 and $Bi_2WO_6/AgInS_2$; XPS characterization of W 4f, O 1s, Ag 3d, Bi 4d, and In 3d; other characterizations of Bi_2WO_6 and $Bi_2WO_6/AgInS_2$; UV−vis spectra of Bi_2WO_6 and $Bi_2WO_6/AgInS_2$; electrochemical characterizations of the PEC biosensor; optimization of experimental conditions; calibration curve; performance comparison with other methods; and spike-and-recovery experiments (PDF)

■ AUTHOR INFORMATION

Corresponding Authors

Yueyun Li − *School of Chemistry and Chemical Engineering, Shandong University of Technology, Zibo 255049, P. R. China;* orcid.org/0000-0001-8558-3863; Email: liyueyun71@163.com

Qin Wei − *Collaborative Innovation Center for Green Chemical Manufacturing and Accurate Detection, Key Laboratory of Interfacial Reaction & Sensing Analysis in Universities of Shandong, School of Chemistry and Chemical Engineering, University of Jinan, Jinan 250022, P. R. China;* orcid.org/0000-0002-3034-8046; Email: sdjndxwq@163.com

Authors

Shanghua Liu − *School of Chemistry and Chemical Engineering, Shandong University of Technology, Zibo 255049, P. R. China; Collaborative Innovation Center for Green Chemical Manufacturing and Accurate Detection, Key Laboratory of Interfacial Reaction & Sensing Analysis in Universities of Shandong, School of Chemistry and Chemical Engineering, University of Jinan, Jinan 250022, P. R. China*

Yue Jia − *Collaborative Innovation Center for Green Chemical Manufacturing and Accurate Detection, Key Laboratory of Interfacial Reaction & Sensing Analysis in Universities of Shandong, School of Chemistry and Chemical Engineering, University of Jinan, Jinan 250022, P. R. China*

Hui Dong − *School of Chemistry and Chemical Engineering, Shandong University of Technology, Zibo 255049, P. R. China*

Xiaodong Yu − *School of Chemistry and Chemical Engineering, Shandong University of Technology, Zibo 255049, P. R. China*

Dao-Peng Zhang − *School of Chemistry and Chemical Engineering, Shandong University of Technology, Zibo 255049, P. R. China*

Xiang Ren − *Collaborative Innovation Center for Green Chemical Manufacturing and Accurate Detection, Key Laboratory of Interfacial Reaction & Sensing Analysis in Universities of Shandong, School of Chemistry and Chemical Engineering, University of Jinan, Jinan 250022, P. R. China;* orcid.org/0000-0002-4321-4282

Complete contact information is available at: https://pubs.acs.org/10.1021/acs.analchem.0c02804

Notes

The authors declare no competing financial interest.

https://dx.doi.org/10.1021/acs.analchem.0c02804
Anal. Chem. 2020, 92, 10935−10939

■ ACKNOWLEDGMENTS

This work is supported by the Key Research and Development Program of Shandong Province (Grant No. 2018GSF120001), the National Key Scientific Instrument and Equipment Development Project of China (Grant No. 21627809); National Natural Science Foundation of China (Grant No. 21777056); and Special Foundation for Taishan Scholar Professorship of Shandong Province.

■ REFERENCES

(1) Zhao, W. W.; Xu, J. J.; Chen, H. Y. *Chem. Soc. Rev.* **2015**, *44* (3), 729−741.
(2) Zhao, W. W.; Xu, J. J.; Chen, H. Y. *Anal. Chem.* **2018**, *90* (1), 615−627.
(3) Shu, J.; Tang, D. P. *Anal. Chem.* **2020**, *92* (1), 363−377.
(4) Zhao, M.; Chen, A. Y.; Huang, D.; Chai, Y. Q.; Zhuo, Y.; Yuan, R. *Anal. Chem.* **2017**, *89* (16), 8335−8342.
(5) Jiang, Z.; Liang, X.; Zheng, H.; Liu, Y.; Wang, Z.; Wang, P.; Zhang, X.; Qin, X.; Dai, Y.; Whangbo, M.-H.; Huang, B. *Appl. Catal., B* **2017**, *219*, 209−215.
(6) Zhang, L. S.; Wang, H. L.; Chen, Z. G.; Wong, P. K.; Liu, J. S. *Appl. Catal., B* **2011**, *106* (1−2), 1−13.
(7) Sun, S.; Wang, W. *RSC Adv.* **2014**, *4* (88), 47136−47152.
(8) Shaw, J. B.; Li, W. Z.; Holden, D. D.; Zhang, Y.; Griep-Raming, J.; Fellers, R. T.; Early, B. P.; Thomas, P. M.; Kelleher, N. L.; Brodbelt, J. S. *J. Am. Chem. Soc.* **2013**, *135* (34), 12646−12651.
(9) Zhao, C.-Q.; Ding, S.-N. *Coord. Chem. Rev.* **2019**, *391*, 1−14.
(10) Wang, X. W.; Sun, G. Z.; Routh, P.; Kim, D. H.; Huang, W.; Chen, P. *Chem. Soc. Rev.* **2014**, *43* (20), 7067−7098.
(11) Zheng, H. Y.; Li, Y. J.; Liu, H. B. A.; Yin, X. D.; Li, Y. L. *Chem. Soc. Rev.* **2011**, *40* (9), 4506−4524.
(12) Kida, T.; Furuso, H.; Kumamoto, K.; Pramata, A. D.; Yuasa, M.; Shimanoe, K. *Chem. - Eur. J.* **2015**, *21* (20), 7462−7469.
(13) Li, J.; Lin, X.; Zhang, Z.; Tu, W.; Dai, Z. *Biosens. Bioelectron.* **2019**, *126*, 332−338.
(14) Kameyama, T.; Takahashi, T.; Machida, T.; Kamiya, Y.; Yamamoto, T.; Kuwabata, S.; Torimoto, T. *J. Phys. Chem. C* **2015**, *119* (44), 24740−24749.
(15) Zhao, W. W.; Ma, Z. Y.; Yan, D. Y.; Xu, J. J.; Chen, H. Y. *Anal. Chem.* **2012**, *84* (24), 10518−10521.
(16) Yin, H. S.; Wang, M.; Zhou, Y. L.; Zhang, X. Y.; Sun, B.; Wang, G. H.; Ai, S. Y. *Biosens. Bioelectron.* **2014**, *53*, 175−181.
(17) Wang, Y. L.; Cui, Y. Y.; Zhao, Y. L.; Liu, R.; Sun, Z. P.; Li, W.; Gao, X. Y. *Chem. Commun.* **2012**, *48* (6), 871−873.
(18) Cui, Y. Y.; Wang, Y. L.; Liu, R.; Sun, Z. P.; Wei, Y. T.; Zhao, Y. L.; Gao, X. Y. *ACS Nano* **2011**, *5* (11), 8684−8689.
(19) Yang, H.; Gurgel, P. V.; Williams, D. K.; Bobay, B. G.; Cavanagh, J.; Muddiman, D. C.; Carbonell, R. G. *J. Mol. Recognit.* **2009**, *23* (3), 271−82.
(20) Jia, Y.; Yang, L.; Feng, R.; Ma, H.; Fan, D.; Yan, T.; Feng, R.; Du, B.; Wei, Q. *ACS Appl. Mater. Interfaces* **2019**, *11* (7), 7157−7163.
(21) Zhang, Y.; Zhang, N.; Tang, Z.-R.; Xu, Y.-J. *Chem. Sci.* **2013**, *4* (4), 1820−1824.
(22) Luo, S.; Ke, J.; Yuan, M. Q.; Zhang, Q.; Xie, P.; Deng, L. D.; Wang, S. B. *Appl. Catal., B* **2018**, *221*, 215−222.
(23) Pei, Y.; Li, X. G.; Chu, H.; Ge, Y. C.; Dong, P.; Baines, R.; Pei, L. Y.; Ye, M. X.; Shen, J. F. *Talanta* **2017**, *165*, 44−51.
(24) Bhoi, Y. P.; Mishra, B. G. *Chem. Eng. J.* **2017**, *316*, 70−81.
(25) Schaal, P. A.; Besmehn, A.; Maynicke, E.; Noyong, M.; Beschoten, B.; Simon, U. *Langmuir* **2012**, *28* (5), 2448−2454.
(26) Low, J.; Yu, J.; Jaroniec, M.; Wageh, S.; Al-Ghamdi, A. A. *Adv. Mater.* **2017**, *29* (20), 1601694.

https://dx.doi.org/10.1021/acs.analchem.0c02804
Anal. Chem. 2020, 92, 10935−10939